Inductance Analysis of Electric Machines by Classical and Numerical Methods

J.J. Germishuizen
Siemens Mobility GmbH
Nürnberg, Germany
Email: johannes.germishuizen@siemens.com

T.J.E. Miller
Emeritus Professor
University of Glasgow
United Kingdom
Email: tjem@retrospeed.co.uk

Keywords

≪AC Machine≫, ≪Finite-element analysis≫, ≪Impedance analysis≫.

Abstract

In electric machine design calculations, strong compatibility is essential between the methods used to design windings, the equivalent circuit model, and the overall electromagnetic performance. This paper presents a structured classification of complementary methods to achieve a unified approach, with particular focus on inductance calculations using classical and finite-element methods.

Introduction

Computer-aided design is now by far the preferred tool for the development of electric machines. Together with advances in materials and manufacturing methods, numerical analysis has helped to increase efficiencies and power densities, to advance the art of motion control, and even to introduce new types of machines such as superconducting machines, permanent-magnet machines of unprecedented size and power density, axial-flux machines, nano-scale machines, and others.

The fundamental theory of the electric machine is rooted in certain definite precepts related to its equivalent-circuit impedances, including generated EMF in some cases. The equivalent circuit is necessarily a *circuit* representation of the machine, since the machine is connected to an external supply circuit and controlled as a circuit element by other circuit elements such as switches and inverters. Internally, however, it is represented by different kinds of model: for example, an equivalent-circuit model and a field model, or a set of field models comprising thermal and electromagnetic fields.

The classical equivalent-circuit model and its parameters are not automatically compatible with the finite-element model. Indeed the dichotomy between "circuit models" and "field models" is very old, and pre-dates modern numerical analysis by many years. But the question of compatibility and the "working together" of these methods is now acute, because both models are essential to the modern designer: numerical analysis for its accuracy and its ability to solve nonlinear problems with complex geometry (including time-dependent problems), and classical theory for its structure and its role in the synthesis of windings, machine configurations, terminal behaviour, and the general understanding of performance.

This paper presents a structure of inductance calculations by different methods, intended to exploit the strengths of both sets of models with the highest possible degree of compatibility, avoiding conflicts, duplication, and wasted effort on inappropriate methods. The structure follows the classical partition of inductances into components, while taking the further step of capturing the effect of magnetic saturation by means of the finite-element method. An important distinction is made between "whole machine" parameters, which belong to the "terminal" equivalent-circuit model, and "partitioned components".

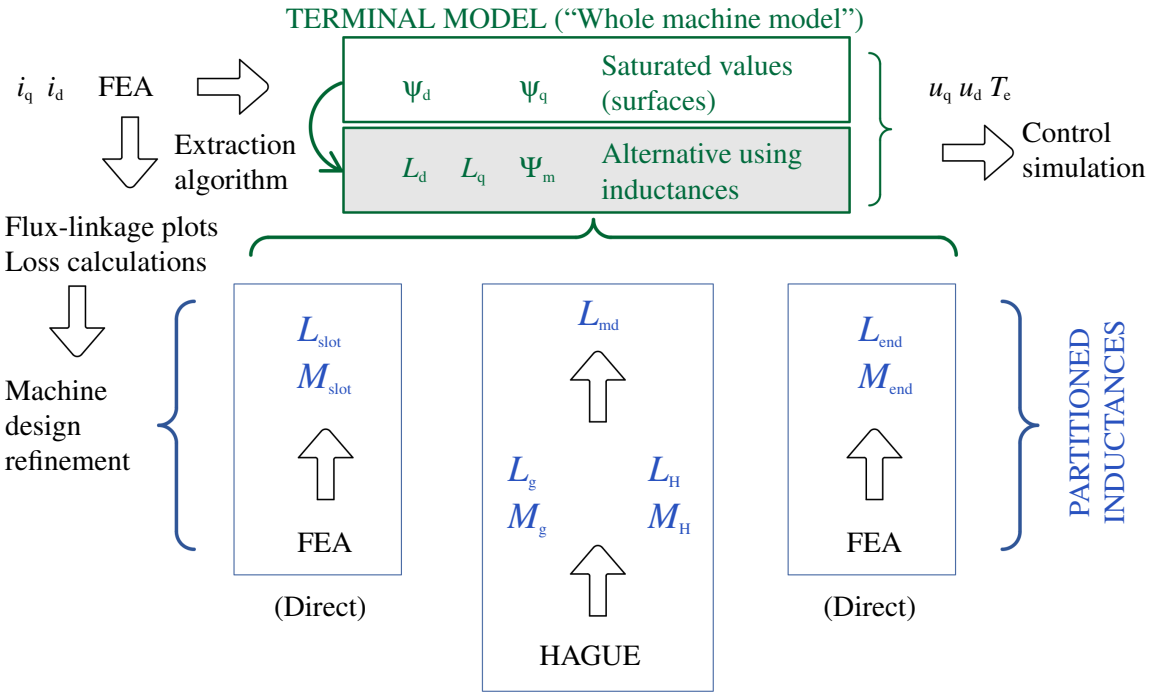

Fig. 1: “Road-map” or structure of inductance calculations

These two classes of parameters are generally used for different purposes and by different engineers, so it is helpful – almost essential – to have them sorted in a definite structure or scheme.

Although the methods described are not in themselves entirely new, the comprehensive treatment of the different methods is rare. The most original aspect is the emergence of quite categorical conclusions about the accuracy, compatibility, and convenience of the different methods and the relationships between them. The presentation of the air-gap magnetizing inductance and the components of harmonic leakage directly from Hague’s solution for a “large-airgap” configuration is also rare, and has not been presented before in a comparison with traditional narrow-gap formulations and finite-element methods. Further, the prediction of induced saliency in a surface-magnet motor is not known to have been published before, while the “extraction algorithm” for the synchronous inductances is shown to be equally suitable for the nonsalient-pole machine and the salient-pole machine.

This paper is essentially a theoretical comparison of calculation methods, and we would make the unusual argument that physical test results would not help to clarify the methods. All the calculation methods are known from wide experience to provide accurate results when used in appropriate circumstances, while the differences between calculation methods are in many cases less than the errors that arise in ordinary physical measurements. Actual physical measurements are possible only in the case of the terminal inductances and not in the case of the components, and even then, inductance measurements are performed relatively less often than for other parameters (such as torque, efficiency, temperature rise, or even resistance) [11, 12]. And while we could not advance the finite-element method as a substitute for physical test, we certainly would hold it up as a standard of accuracy in calculation.

Structure of inductance calculations

The proposed structure is shown in Fig. 1, and it can be viewed as a “road-map” in the sense that it suggests or prescribes “best practice” methods for the calculation of the various inductances and their components.

A simple but general concept of the equivalent circuit is shown in Fig. 2, in which EMFs and impedances are combined in a circuit of greater or lesser complexity. Fig. 2 shows the beginnings of the partition of EMFs and inductances into “fundamental” and “harmonic” components, which are generally attributable

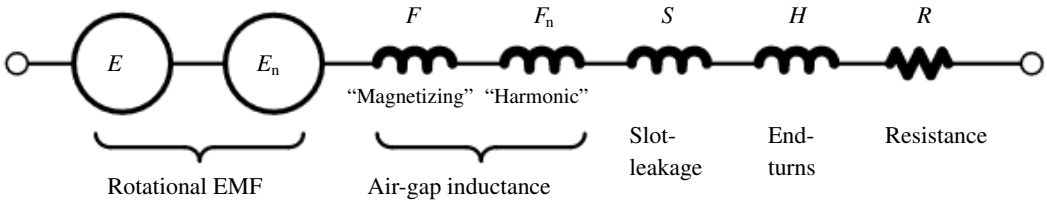

Fig. 2: General concept of equivalent circuit

to the space-harmonic properties of the winding distribution. A single circuit is usually sufficient for non- salient-pole machines, while a double circuit is needed for salient-pole machines such as the interior permanent-magnet motor (IPM), the wound-field synchronous motor, or the synchronous reluctance motor. In AC machines where the focus is on steady-state performance, the EMFs and impedances in Fig. 2 are usually invariant in time, but liable to saturation as a function of current and/or the strength of the excitation (magnets or field current).

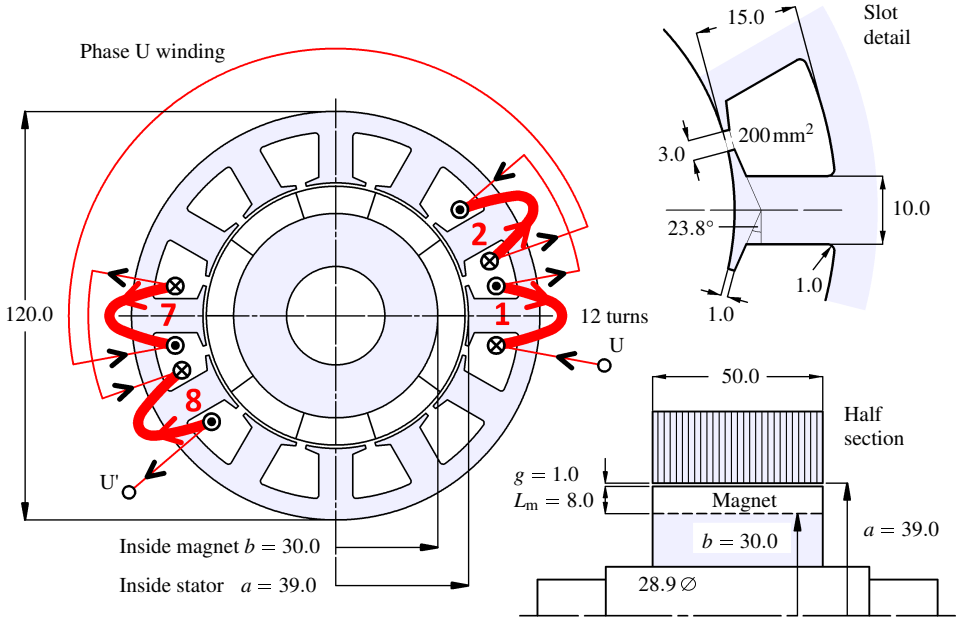

Fig. 3: Example surface-magnet PM brushless AC motor [14]

Example – a surface-magnet PM motor

At this point it may be helpful to introduce an example motor, Fig. 3. While this class of motor can be viewed as simpler than the IPM or the induction motor, it does in fact have *all* the inductance components necessary to illustrate *all* the methods of calculation, including the effects of saturation and even a small degree of saliency.

Table I shows the results of the inductance calculations.

Components and Methods

A key distinction in Fig. 1 is to separate the inductance parameters into "terminal" inductances and "partitioned" inductances. These are used for different purposes, and even by different engineers, as is suggested in the right-hand column of Table I. From an external viewpoint, the terminal inductances are

Table I: Inductance analysis

Component	Partitioned FEA	Partitioned Hague	Partitioned MEC	Description	Main function
L_{d}	0.2555	0.2815	0.2366	Synchronous d	CSP
L_{q}	0.2368	0.2815	0.2366	Synchronous q	CSP
L_{ph}	0.2489	0.2554	0.2160	Phase self	TM
M_{ph}	−0.0263	−0.0261	−0.0206	Phase mutual	TM
L_{md}		0.055 32	0.043 56	Magnetizing	DMD
L_{g}		0.1354	0.0857	Air-gap self	W
M_{g}		−0.0106	0	Air-gap mutual	W
$L_{\mathrm{g\ \&\ slot}}$	0.2424	0.024 89		2D self	W
$M_{\mathrm{g\ \&\ slot}}$	−0.0263	0.0261		2D mutual	W
L_{g5}		0.036 88		5^{th} harmonic self	W
M_{g5}		−0.018 44		5^{th} harmonic mutual	W
L_{H}		0.090 71		Harmonic	W
L_{slot}	0.1238		0.1238	Slot self	DMD
M_{slot}	−0.0206		−0.0206	Slot mutual	DMD
L_{end}			0.0065	End-winding	DMD

W = winding design; **TM** = test & measurement; **DMD** = detailed machine design; **CSP** = control, simulation, performance

obviously of key importance, and this is reflected in Table I where the synchronous inductances L_{d} and L_{q} are highlighted all the way across the table – in other words, regardless of the method used to calculate them. L_{ph} and M_{ph} fall into the same category.

The pre-eminence given to L_{d} and L_{q} presupposes a terminal model in dq axes, because this is by far the most common circumstance for this type of machine, indeed for any inverter-fed machine. On the other hand, if direct phase variables are used, the phase inductances L_{ph} and M_{ph} (self and mutual) would be the natural ones to use. In salient-pole machines, of course these are rotor-position-dependent, and (as is well known) the basic reason for transforming to dq axes is to eliminate this dependence.

These important inductances L_{d} and L_{q} can be calculated directly and accurately using the finite-element method, no matter how much they are affected by saturation. Fig. 4 shows the result for the example motor; the flux-linkages ψ_{d} and ψ_{q} are presented as functions of the currents i_{d} and i_{q} [13, 12].

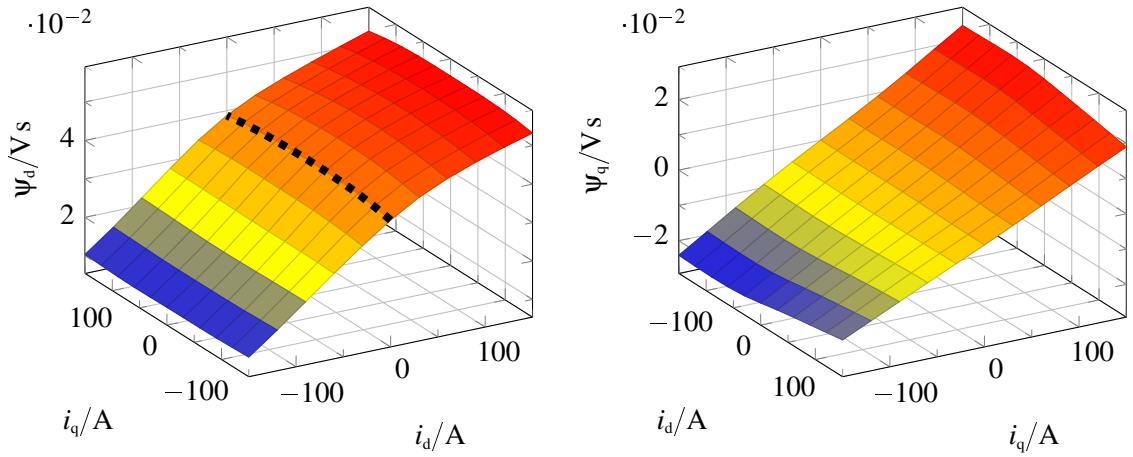

(a) d-axis flux linkage ($B_{\mathrm{r}} = 1.2\,\mathrm{T}$)

(b) q-axis flux linkage ($B_{\mathrm{r}} = 1.2\,\mathrm{T}$)

Fig. 4: Flux-linkage surfaces of ψ_{d} and ψ_{q} calculated by the finite-element method

Although L_{d} and L_{q} can be calculated from the assembly of components by the other methods in the

"partitioned" category, this method is generally less accurate.

However, the magnetizing inductance L_{md} should be singled out for consideration because it forms an important link between the terminal model and the partitioned model. It is also one of the central parameters in the theory of winding configurations. It can be defined as that component of L_{d} that is attributable to the air-gap flux produced by the fundamental space-harmonic of the winding distribution (with all three phases acting together), and it can be calculated for the example motor by (1) derived from the original analysis of Hague [9, 10]. (See also [7, 8]).

$$L_{\mathrm{md}} = \frac{3}{2} k_{\mathrm{w}} T_{\mathrm{ph}} \Phi_{\mathrm{a1}} = \frac{6\mu_0 L_{\mathrm{stk}} (k_{\mathrm{w}} T_{\mathrm{ph}})^2}{\pi p} \left[\frac{(a/b)^{2p} + 1}{(a/b)^{2p} - 1} \right] \quad \mathrm{mH}. \tag{1}$$

The form of this equation shows its usefulness in machine design, containing as it does the fundamental winding factor k_{w}, the turns in series per phase T_{ph}, the number of pole-pairs p, the radial dimensions a, b and the stack length L_{stk}. Yet L_{md} cannot be calculated directly by the finite-element method, because it requires a harmonic analysis of the winding distribution *and* the separation of the air-gap flux from all other flux components such as slot-leakage, end-winding leakage, and harmonics.

Hague's method is the pure harmonic analysis of an ampere-conductor distribution on the surface of a smooth cylinder. This method and the finite-element method are complementary. In other words, what one method does, the other does not. When the slot-leakage and end-winding leakage are added to the air-gap component, the two methods do everything needed, and agree closely in the unsaturated case.

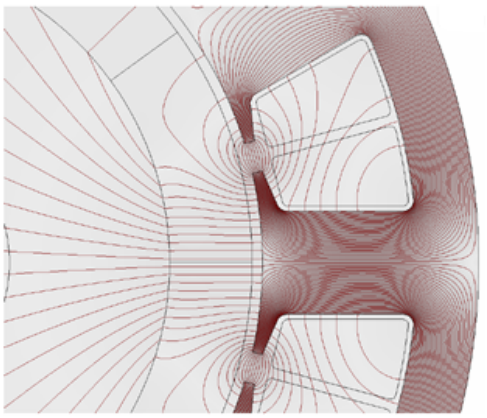

Fig. 5: Slot leakage [15]

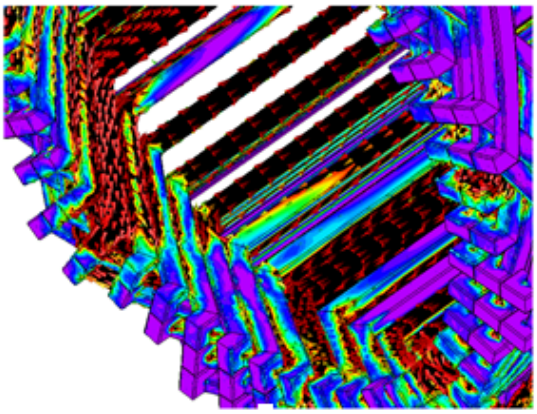

Fig. 6: 3D eddy-currents [15]

Fig. 5 shows the calculation of inductance by the finite-element method. The classical magnetic-equivalent-circuit (MEC) method assumes often that the flux excited by current in the slot goes across the slot, with flux-lines everywhere perpendicular to the slot centre-line. That this is far from reality is immediately clear in Fig. 5. The MEC method often underestimates the slot-leakage inductance by a significant amount (although to be fair, this has been recognized and allowed for in many cases, [1, 2, 3, 4, 5]).

Fig. 6 shows a 3D eddy-current calculation in the end-region of an AC motor stator – one of the most sophisticated instances of modern numerical analysis. In simple terms the end-winding inductance would be obtained from a magnetostatic version of this calculation. This figure is included to underline the power of the FEA method in 3D calculations with time-dependent fields, while magnetic saturation is included in the formulation in both Figs. 5 and 6. This type of calculation is not possible with any serious level of accuracy or robustness by means of traditional methods (although of course the classical approximations are quick and still widely used).

The terminal or "whole machine" model

We return now to the "whole machine" or "terminal" model to consider how it may be efficiently calculated (without any partitioning); how it is used; and the effect of saturation [14]. The model is expressed

in the classical Park's equations

$$\begin{aligned} u_{\mathrm{d}} &= R_1 \cdot i_{\mathrm{d}} - \omega \cdot \psi_{\mathrm{q}} \\ u_{\mathrm{q}} &= R_1 \cdot i_{\mathrm{q}} + \omega \cdot \psi_{\mathrm{d}} \end{aligned} \tag{2}$$

from which the phasor or r.m.s. terminal voltage is obtained as

$$U_{1,\mathrm{phase}} = \sqrt{\frac{u_{\mathrm{d}}^2 + u_{\mathrm{q}}^2}{2}} \quad V_{\mathrm{r.m.s.}}. \tag{3}$$

The torque equation is used at the same time in the form

$$T_{\mathrm{e}} \;=\; \frac{m}{2} \cdot p \cdot (\psi_{\mathrm{d}} \cdot i_{\mathrm{q}} - \psi_{\mathrm{q}} \cdot i_{\mathrm{d}}) \,. \tag{4}$$

When the motor is fed by a current-regulated PWM inverter, the current and phase angle are controlled to have specific values i_{d} and i_{q}. For "sinewave" machines an efficient finite-element solution can be obtained at a fixed rotor position, for example when the d-axis is aligned with phase U, $\theta = 0$. By Park's inverse transformation the instantaneous phase currents to be used in the finite-element formulation then have the fixed values

$$\begin{aligned} i_{\mathrm{u}} &= i_{\mathrm{d}} \cos(\theta) - i_{\mathrm{q}} \sin(\theta) = i_{\mathrm{d}}; \\ i_{\mathrm{v}} &= i_{\mathrm{d}} \cos(\theta - 120^\circ) - i_{\mathrm{q}} \sin(\theta - 120^\circ) = -\frac{1}{2} i_{\mathrm{d}} + \frac{\sqrt{3}}{2} i_{\mathrm{q}}; \\ i_{\mathrm{w}} &= i_{\mathrm{d}} \cos(\theta + 120^\circ) - i_{\mathrm{q}} \sin(\theta + 120^\circ) = -\frac{1}{2} i_{\mathrm{d}} - \frac{\sqrt{3}}{2} i_{\mathrm{q}}; \end{aligned} \tag{5}$$

The finite-element calculation produces the phase flux-linkages ψ_{u}, ψ_{v}, ψ_{w} from which ψ_{d} and ψ_{q} are obtained by Park's transformation. This completes the description of a "whole machine" terminal model in which the circuit equations are perfectly integrated with the finite-element method. The necessary finite-element data is shown in Fig. 4 in the form of flux-linkage surfaces computed for ψ_{d} and ψ_{q} over a range of currents i_{d} and i_{q} for the example motor in Fig 3. The data in these surfaces completely characterizes the motor at the terminals, making it possible to calculate the torque and the required fundamental terminal voltage at any load or speed; this data is thus in a form suitable for immediate integration with a field-oriented control scheme.

Fig. 4 shows the calculations in which the magnet remanent flux-density has its normal value (1.2 T). The surfaces show the variation in the saturation level caused by the variation in *current*; of course they include the effect the magnets as well. The actual flux-linkage/current relationships are of the form $\psi_{\mathrm{d}} = \psi_{\mathrm{d}}(i_{\mathrm{d}}, i_{\mathrm{q}})$ and $\psi_{\mathrm{d}} = \psi_{\mathrm{d}}(i_{\mathrm{d}}, i_{\mathrm{q}})$, described by the surfaces in Fig. 4. Because of the magnetic nonlinearity, it is not possible to resolve or segregate the saturation effects *uniquely* into separate components attributable to the current and the magnet. However, a common form used for segregation is

$$\begin{aligned} \psi_{\mathrm{d}} &= \Psi_{\mathrm{m}}(i_{\mathrm{q}}) + L_{\mathrm{d}} \cdot i_{\mathrm{d}}; \\ \psi_{\mathrm{q}} &= L_{\mathrm{q}} \cdot i_{\mathrm{q}} \end{aligned} \tag{6}$$

where L_{d} and L_{q} are the synchronous inductances in the d- and q-axes, and Ψ_{m} is the flux-linkage per phase produced by the magnet. It is shown here as a function of i_{q}, to recognize the effect of cross-saturation (which is particularly strong in the IPM). In general, Ψ_{m} is a function of both i_{d} and i_{q}, although it is common to take it as constant equal to the open-circuit value. Furthermore, in the most general case L_{d} and L_{q} are functions of both i_{d} and i_{q} to a greater or lesser extent. Only in the case of a magnetically linear machine is it possible to define *unique* constant values of Ψ_{m}, L_{d} and L_{q}.

Extraction of inductance and identification of saturation effects – In routine design calculations it is

necessary to have an 'extraction' algorithm to obtain working values of Ψ_m, L_d and L_q, especially when these values are required in the design of field-oriented controllers. A review of the literature shows that many such algorithms or procedures are in use, but it is not essential to standardize them as long as consistent results are obtained within one company. (See, for example, [13, 12]).

The surface-magnet motor in Fig. 3 is often considered to be "simple" and free from saturation effects, in contrast with the IPM which has very strong and variable saturation effects. However, finite-element analysis shows that saturation due to the *magnet* can be significant. This result appears immediately from the comparison of L_d and L_q values in Table I. L_d falls to 91 % and L_q to 84 % of the unsaturated values which can be attributed, at least in part, to the small saturated regions in the rotor hub just inside the magnets. We can identify this as "induced saliency".

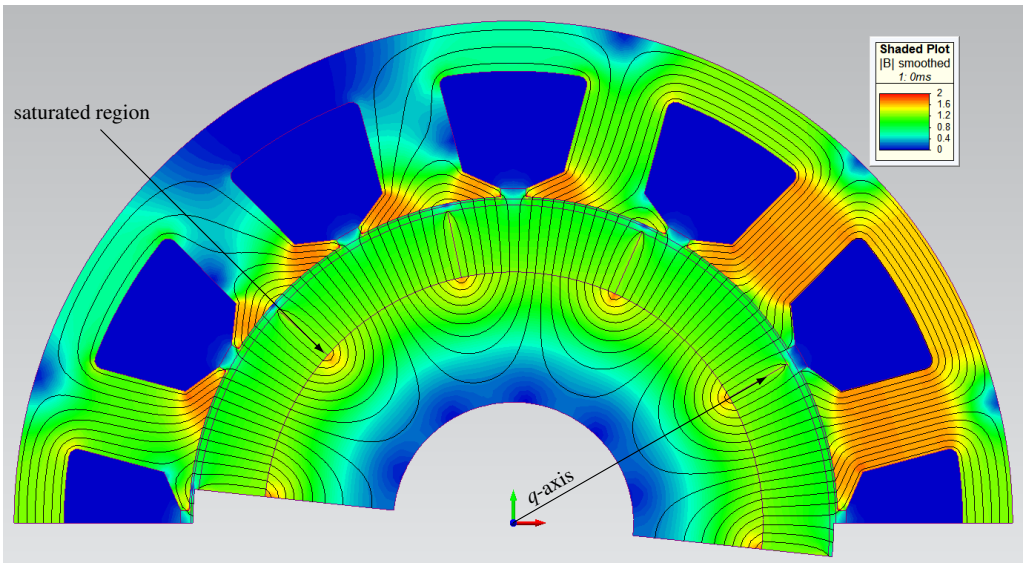

Fig. 7: Finite-element flux-plot showing "induced saliency"

It is natural to ask where the saturation effects are located – in which parts of the magnetic circuit? For the purpose of creating a simulation model to be used with control-system simulations, this question could be seen as irrelevant, on the grounds that the saturated terminal model of (2)-(4), together with the surfaces in Fig. 4, are completely adequate.

However, the machine *designer* is faced with the challenges of alleviating saturation effects as far as possible, and the immediate resource to be used for this is the flux-plot, an example of which appears in Fig. 5. It is often possible to tell at a glance, whether a tooth-width or a yoke section is too narrow, and remedial action can be taken very quickly in the CAD environment. The finite-element method provides many other tools for the assessment of design dimensions, for example the calculation of local loss densities.

But the flux-plot and related intensity maps do not answer all the designer's questions. For example, the slot-leakage inductance is a significant component (not greatly affected by saturation), and its value should be worked out in the process of optimizing both the slot shape and the winding pattern. Likewise the air-gap inductance needs to be separated into its space-harmonic components, again in relation to the winding pattern. Both these inductance components have self- and mutual components between phases, which are relevant to the design of the winding layout. The value of the separate inductance components gradually becomes clear, whether they are saturated or not.

The total terminal inductances can be expressed as a sum [14],

$$L_d \cong L_q = L_{md} + \overbrace{(L_{diff} - M_{diff})}^{L_H} + (L_{slot} - M_{slot}) + (L_{end} - M_{end}) \tag{7}$$

where L_{md} is that part of the synchronous inductance attributable to the space-harmonic of the winding at the working harmonic; L_H is the harmonic or differential leakage inductance; and L_{slot}, M_{slot}, L_{end} and M_{end} are the self- and mutual slot-leakage and end-winding leakage inductances. Not only the individual values, but also the balance between these components is important.

If, then, we imagine starting with the "whole machine" terminal inductances in Table I and moving into the "partitioned" part of the table, we can begin to seek the most appropriate methods for determining the components. It is not a question of splitting up the finite-element results for the terminal inductances, so much as generating a set of component values from the three main sources in the Table:

- Direct magnetic equivalent-circuit methods [1, 2, 3, 4, 5, 6]
- Hague-type analysis of air-gap fields and their harmonics [9, 10, 7, 8]
- Finite-element calculations on isolated parts of the machine [1, 2]

This structure is expressed in a more generalised way in Fig. 1.

Conclusion

A summary of findings can now be given, based on the comprehensive set of inductance components calculated by the three classes of method and summarized in Table I.

(a) Direct magnetic equivalent-circuit methods are the quickest but also the least accurate, although it is dangerous to make sweeping statements because there is a huge variety of these methods going back over 120 years, often supported or verified by test data.

(b) The Hague-type analysis of the air-gap field and its harmonics is very accurate within the confines of its idealised model. It is especially valuable for the surface-magnet motor in dealing with the air-gap fields (from both the magnet and the winding), while for all machines it is intimately connected with the theory of winding factors. This raises its value in support of the design of windings. It is also very quick, being algebraic in formulation.

(c) Finite-element calculations on isolated parts of the machine are useful only where such isolation is clearly valid: for example, in calculating slot-leakage and end-winding leakage (which is not seriously possible by any other method).

When the results of these methods are put together, we find in particular that the Hague-type methods are generally the best for unsaturated air-gap and harmonic-leakage components, while the finite-element method is the most accurate (but also the slowest) for all the other components.

It therefore becomes possible to treat Fig. 1 as a road-map or classification of methods that helps to choose the most appropriate method for each task; and most importantly, to avoid wasting time on inappropriate methods. The finite-element method is also completely sufficient for the terminal model or "whole machine"model.

We have described a structured "road-map" of design calculation methods for the inductances of inverter-fed electric machines, in which the most appropriate tools are used for the respective components. It is shown that the methods can be applied in a "non-overlapping" manner that maximizes their compatibility, especially in regard to the combination of classical theory and finite-element analysis. Two objectives are achieved without the need to reconcile conflicts in calculated values: (i) providing accurate simulation models for control-system simulation and (ii) producing detailed component data for the refinement of machine designs. The structure includes both the "whole machine" terminal models and the detailed partition of inductance components that is necessary for detailed design and the synthesis and analysis of windings. Saturation of parameters due to currents and/or magnets is included in the "whole machine" model through finite-element methods without the need for artificial simplifying assumptions.

References

[1] A. Boglietti, A. Cavagnino and M. Lazzari: Modelling of the closed rotor slot effects in the induction motor equivalent circuit, International Conference on Electric Machines, ICEM, paper ID 781, 2008, pp. 1-4.

[2] A. Tessarolo: Analytical Determination of Slot Leakage Field and Inductances of Electric Machines With Double-Layer Windings and Semiclosed Slots, IEEE Transactions on Energy Conversion, Vol. 30, No. 4, December 2015, pp. 1528-1536.

[3] M. Bortolozzi, L. Branzo, A. Tessarolo and C. Bruzzese: An Improved Analytical Expression for Computing the Leakage Inductance of a Circular Bar in a Semi-Closed Slot, International Conference on Sustainable Mobility Applications, Renewables and Technology (SMART), 2015, pp. 1-5.

[4] M. Bortolozzi, L. Branzo, A. Tessarolo and C. Bruzzese: Improved Analytical Computation of Rotor Rectangular Slot Leakage Inductance in Squirrel-Cage Induction Motors, International Conference on Sustainable Mobility Applications, Renewables and Technology (SMART), 2015, pp. 1-5.

[5] A.F. Puchstein: Calculation of Slot Constants, AIEE Transactions, Vol. 66, pp. 1315-1323, 1947.

[6] M. Caruso, A.O. Di Tommaso, F. Genduso, R. Miceli and G.R. Galluzzo: A General Mathematical Formulation for the Determination of Differential Leakage Factors in Electrical Machines With Symmetrical and Asymmetrical Full or Dead-Coil Multiphase Windings, IEEE Transactions on Industry Applications, Vol. 54, No. 6, November/December 2018, pp. 5930-5940

[7] A. Hughes and T.J.E. Miller: Analysis of fields and inductances in air-cored and iron-cored synchronous machines, IEE Proceedings Vol. 124, pp. 121-128, 1977.

[8] T.J.E. Miller and A. Hughes: Comparative design and performance analysis of air-cored and iron-cored synchronous machines, IEE Proceedings Vol. 124, pp. 127-132, 1977.

[9] B. Hague: Electromagnetic Problems in Electrical Engineering, Oxford University Press, 1929.

[10] Z.P. Xia: Analytical Magnetic Field Analysis of Halbach Magnetized Permanent-Magnet Machines, IEEE Transactions on Magnetics, Vol. 40, No. 4, July 2004, pp. 1864-1872.

[11] T.J.E. Miller: Methods for testing permanent-magnet AC motors, IEEE Industry Applications Society Annual Meeting, Toronto, pp. 494-499, 1981

[12] T.J.E. Miller, M. Popescu, C. Cossar, M.I. McGilp, M. Olaru, A. Davies, J. Sturgess and A. Sitzia: Embedded Finite-Element Solver for Computation of Brushless Permanent-Magnet Motors, IEEE Transactions on Industry Applications, Vol. 44, No. 4, July/August 2008, pp. 1124-1133.

[13] J. Germishuizen, S. Stanton and V. Delafosse: Integrating FEM in an Everyday Design Environment to Accurately Calculate the Performance of IPM Motors, Studies in Applied Electromagnetics and Mechanics, Vol. 34, 2010, pp. 235-243.

[14] J.R. Hendershot and T.J.E. Miller: Design Studies in Electric Machines, MotorDesignBooks.com, ISBN 978-0-9840687-4-6 (e-Book 978-0-9840687-3-9).

[15] Acknowledgement: Powersys / JSOL Corporation and H. Sano, Figs. 5 and 6; Figs. 1, 2, 3, 5 and 6 and eqns. (1)–(7) are reproduced by kind permission of the authors of Ref. [14].